Proceedings of the 21st ICSMGE, Vienna, Austria, 14 – 19 June 2026. Pistrol, Adam & Schweiger (eds.)
Published by: ÖGG, Austrian Society for Geomechanics, Salzburg, Austria, ISBN 978-3-9503898-4-5
https://doi.org/10.53243/ICSMGE2026-1221

Numerical analysis on ground heave caused by compaction grouting

Lup Wong Wong
SMEC Asia Limited, Hong Kong SAR, China, lupwong.wong@smec.com

ABSTRACT: Compaction grouting has been one of the ground treatment methods for correcting ground movements caused by underground works such as deep excavations and tunnelling. This paper reports the results of parametric studies on the mechanism of ground heave caused by compaction grouting. The numerical analysis adopts the Hardening-soil with small-strain stiffness (HSS) constitution soil model and the 2-Dimensional axis-symmetry finite element model. The spherical cavity expansion method is adopted to simulate the expansion of the grout bulb. The grout injection is simulated by applying radial pressures to the spherical void. Excess pore pressures of 0.7 times the net cavity pressures have been generated during cavity expansion. The parametric study shows that the computed ground heave profiles can be expressed by the Student's T-distribution. The volume of heave is equal to the volume of grout.

KEYWORDS: Grouting pressure, cavity expansion, soil pressure, excess pore pressure, shear stress, heave.

1 INTRODUCTION

Compaction grouting has been the ground improvement method for uplifting structures to rectify settlements caused by excavations. Wong et al. (1996) reported the application of compaction grouting for rectification of building settlements. The uplifting principle is to inject grouting materials beneath the foundation levels. As the grouting pressure increases, the grout body in ground expands, induces ground heaves and uplifts the structures above the grout body. The case that Wong & Chen (1997) reported is one of the case histories for successful application.

On the other hand, these cases were experimental and conducted as trials. Prior to field implementation, its performance was not certain. Due to lacking reliable analytical tools, it would be difficult to explore the mechanism for successful applications. The experience obtained could not be converted to useful guides for reference of future application.

To study the mechanism and the performance of compaction grouting, numerical analysis is conducted and the results are presented herein. The spherical cavity expansion method is used to simulate the injection of a single bulb. Cases with different grout bulb diameters and undrained shear strengths for the surrounding soil are studied. The results of this parametric study will be useful references for future applications.

2 NUMERICAL MODEL

2.1 *Spherical Void Expansion*

The compaction grouting typically injects grout materials below the ground surface for inducing ground heave. In the trial grouting programme that Moh et al. (1994) reported, the compaction grouting injects grout materials in bulbs at the tips of the open-end grout pipes of 100 mm in diameter. After injecting certain volume of grout, lifting the grout pipes by 0.5 m for injection of the next grout bulb follows. In this study, the analysis of ground movements induced by single bulbs of various diameters adopts the spherical void expansion method.

2.2 *Axisymmetric 2-Dimensional Model*

Figure 1 and Figure 2 depict the finite element mesh adopted for numerical analysis. Due to symmetry, the analysis uses a 2-Dimensional model to approximate a 3-Dimensional domain. The spherical grout bulb is composed of a 24-side polygon. The radial pressures applying onto the 24 sides along the interface between the spherical void and the surrounding ground simulates the grout injection.

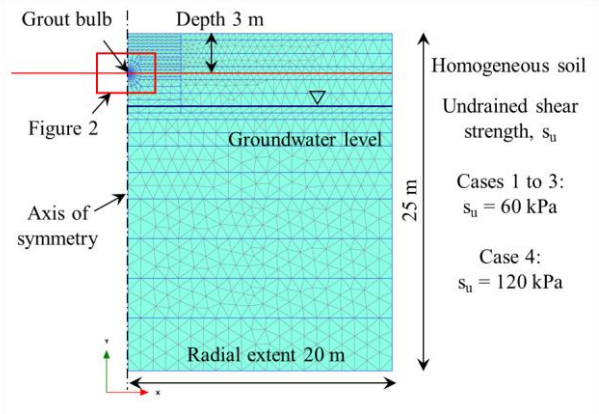

Figure 1. Finite element mesh for numerical analysis on compaction grouting.

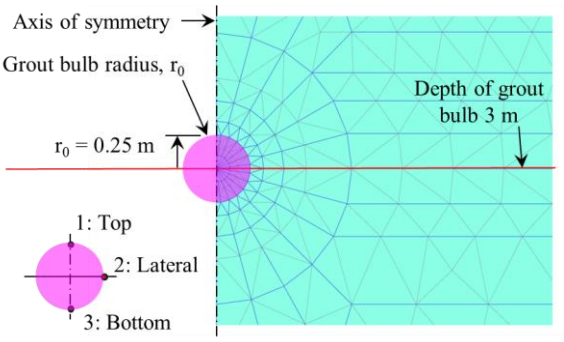

Figure 2. Finite element mesh with a grout bulb of 0.5 m in diameter.

2.3 *Nonlinear Soil Model*

The PLAXIS-2D finite element software developed by PLAXIS BV (2013) has become a popular tool for geotechnical analysis and design. This study adopts the nonlinear Hardening-soil with small-strain stiffness (HSS) constitutive soil model (Benz 2006, Schanz & Vermeer 1998, Schanz et al. 1999) available in the PLAXIS software. Table 1 summarized the stiffness parameters adopted. The undrained shear strengths of 60 kPa and 120 kPa with the Undrained B material, Poisson's ratio υ_{ur} = 0.2 and the earth pressure coefficient K_0 = 1 are adopted.

Table 1. Stiffness parameters for the HSS model.

Soil type	Reference Stiffness, MPa		Initial shear modulus	Reference strain, $\gamma_{0.7}$
	E^{ref}_{50}, E^{ref}_{oed}	E^{ref}_{ur}	G^{ref}_0, MPa	
Clay	15	75	75	0.0005

2.4 *Updated Mesh*

Since compaction grouting induces large magnitude of ground movements, the computation selects the option of updated mesh that available in the PLAXIS software. This option is essential as the deformations of the meshes surrounding the grout bulb would be highly distorted causing discontinuity in the iteration process. The mesh updating after running each stage significantly smoothens the mesh deformation.

2.5 *Analysis Cases*

The analysis comprises 4 cases. Case 1, Case 2 and Case 3 have the initial grout bulb diameters of 0.5 m, 0.7 m and 0.2 m respectively. The undrained shear strength, s_u, that adopted for these 3 cases is 60 kPa. Case 4 that have the bulb diameter of 0.5 m adopts the s_u value of 120 kPa to study the shear strength effects to compaction grouting. The grout bulbs are 3 m in depth. The soil unit weight adopted is 18.6 kN/m^3.

Applying radial cavity pressures, P_c, in stages simulates the spherical expansion. As summarized in Table 2, the pressure increment in each stage is 60 kPa for Case 1 and 13 stages were successfully conducted before the failure in the iteration process. For Case 2, the pressure increment for each stage is 20 kPa and 25 stages were completed.

Table 2. Cases for studying the compaction grouting.

Case	Dia-meter D, m	Undrained shear strength s_u, kPa	Number of stages	Grouting pressure, kPa	
				Stage increment	Final stage
1	0.5	60	13	60	780
2	0.7	60	25	20	500
3	0.2	60	11	60	660
4	0.5	120	20	60	1200

3 SOIL PRESSURES INDUCED BY GROUTING

3.1 *Grouting Pressures versus Computed Volume Strains*

Grouting pressures applying to the spherical void simulates the grout injection process. The initial diameters for the grout bulbs range from 0.2 m to 0.7 m for Case 1 to Case 3. Equations 1 to 3 define the net pressures at the grout-soil interface as:

$$P_{c\text{-}net} = P_c - \sigma_{r0} \quad (1)$$

$$\sigma_{r\text{-}net} = \sigma_r - \sigma_{r0} \quad (2)$$

$$\sigma'_{r\text{-}net} = \sigma'_r - \sigma'_{r0} \quad (3)$$

where: $P_{c\text{-}net}$ is the applied net grouting pressure, $\sigma_{r\text{-}net}$ and $\sigma'_{r\text{-}net}$ are the net total and the net effective radial pressures respectively, σ_r and σ'_r are the total and the effective radial pressures respectively, σ_{r0} and σ'_{r0} are the initial total and the initial effective radial pressures respectively induced at the grout-soil interface.

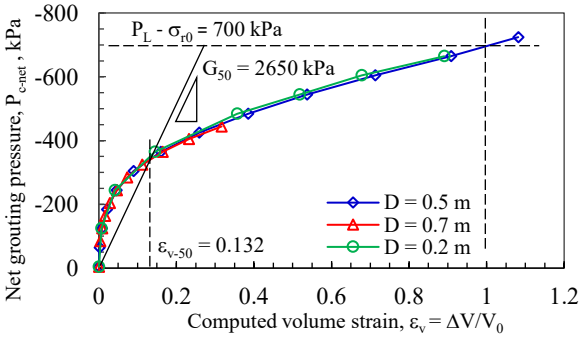

Figure 3. Grouting pressures versus volume strains.

The computed volume of grout injected, ΔV, normalized with the initial volume of the spherical void, V_0, is the volume strain, $\Delta V/V_0 = \varepsilon_v$, of the surrounding soil. Figure 3 presents the computed volume strains versus the applied $P_{c\text{-}net}$ values for Case 1 to Case 3 and shows that variation in the bulb diameters does not affect the $P_{c\text{-}net}$ versus the $\Delta V/V_0$ relationship. The size effect of the grout bulbs to compaction grouting is negligible.

3.2 *Pressures at Grout-soil Interface – Case 1*

Figure 4 presents the computed soil pressures at the grout-soil interface in response to the $P_{c\text{-}net}$ values for Case 1, which has the grout bulb diameter of 0.5 m. The σ_{r0} is 55.8 kPa at 3 m depth. Figures 4(a), 4(b) and 4(c) present the computed $\sigma_{r\text{-}net}$, the excess pore pressures, ΔU, and the computed $\sigma'_{r\text{-}net}$ values respectively at Point 1 to Point 3 along the grout-soil interface that defined in Figure 2.

For the $P_{c\text{-}net}$ values below 304 kPa, the $\sigma_{r\text{-}net}$, the ΔU and the $\sigma'_{r\text{-}net}$ values are proportional to the $P_{c\text{-}net}$ values. The $\sigma_{r\text{-}net}/P_{c\text{-}net}$ ratio is 1, the $\Delta U/P_{c\text{-}net}$ ratio is 0.7 and the $\sigma'_{r\text{-}net}/P_{c\text{-}net}$ ratio is around 0.3. For the $P_{c\text{-}net}$ values exceeding 304 kPa, Figure 4(c) shows that the $\sigma'_{r\text{-}net}$ reaches an ultimate value, $(\sigma'_{r\text{-}net})_{ult}$, of 82 kPa. As shown in Figure 8, the surrounding soil starts reaching the ultimate shear stress of 60 kPa at the $P_{c\text{-}net}$ value of 304 kPa.

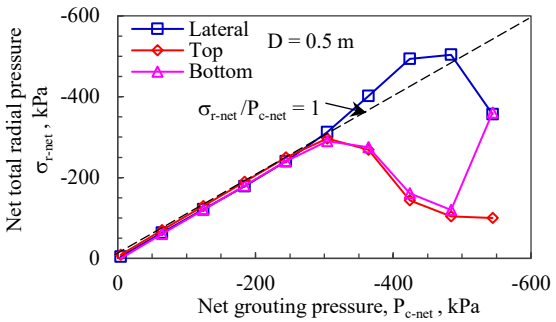

(a) Total radial pressures.

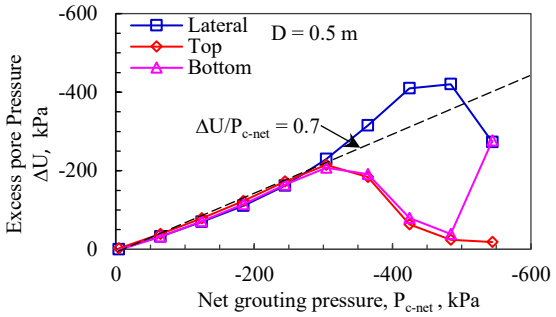

(b) Excess pore pressures.

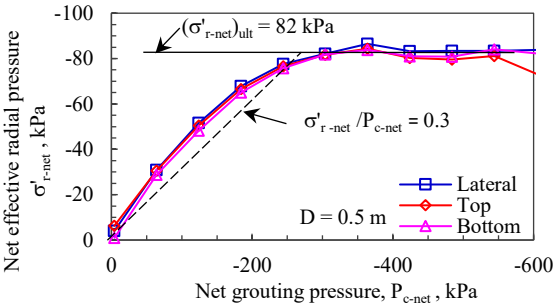

(c) Effective radial pressures.

Figure 4. Computed soil pressures at the grout-soil interface - Case 1.

Generation of excess pore pressures plays a dominating role in the performance of compaction grouting. Although the grout bulb is above the groundwater level, generation of ΔU occurs due to dilation or contraction of the undrained saturated soil upon shearing. Figure 4(b) shows that at the $P_{c\text{-net}}$ values exceeding 304 kPa, generation of positive pore pressures occurs at the lateral Point 2 and generation of negative pore pressures occurs at the upper Point 1 and the lower Point 3 along the grout-soil interface. Such pore pressures response is the indication of contraction and dilation of the surrounding soil.

3.3 *Pressures at Grout-soil Interface – Case 2*

Figures 5(a), 5(b) and 5(c) present the computed soil pressures, the $\sigma_{r\text{-net}}$, ΔU and $\sigma'_{r\text{-net}}$ values, in response to the various $P_{c\text{-net}}$ values for Case 2. For the $P_{c\text{-net}}$ values less than 244 kPa, the computed $\sigma_{r\text{-net}}$, ΔU and $\sigma'_{r\text{-net}}$ values are proportional to the $P_{c\text{-net}}$ values. The $\sigma_{r\text{-net}}/P_{c\text{-net}}$ ratio is 1, the $\Delta U/P_{c\text{-net}}$ ratio is 0.7 and the $\sigma'_{r\text{-net}}/P_{c\text{-net}}$ ratio is around 0.3.

For the $P_{c\text{-net}}$ values exceeding 244 kPa, Figure 5(b) shows the generation of negative pore pressures at the upper, the lateral and the lower points of the grout-soil interface. Such pore pressures response is the indication of dilation of the soil surrounding the grout bulb. Like Case 1, Figure 5(c) shows that the $\sigma'_{r\text{-net}}$ reaches an ultimate value, $(\sigma'_{r\text{-net}})_{ult}$, of 82 kPa for the $P_{c\text{-net}}$ values exceeding 244 kPa.

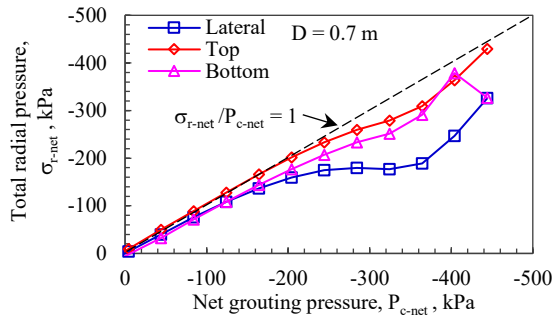

(a) Total radial pressures.

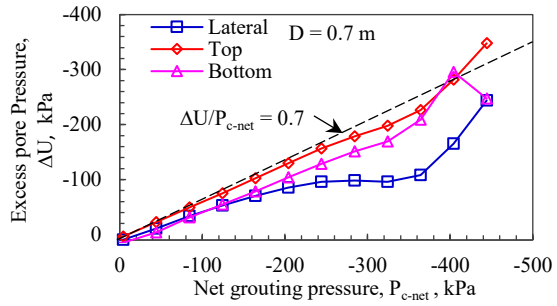

(b) Excess pore pressures.

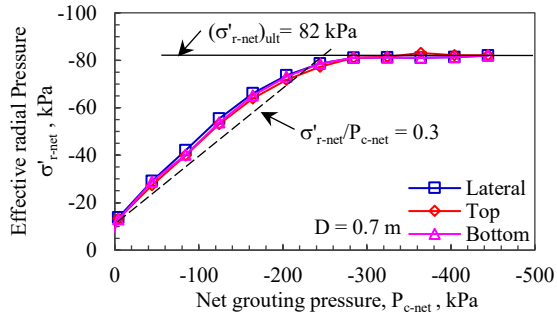

(c) Effective radial pressures.

Figure 5. Computed soil pressures at the grout-soil interface - Case 2.

3.4 *Variation of Pressures with Radial Distances*

Figure 6 presents the variation of the $\sigma_{r\text{-net}}$ and the ΔU along the horizontal radial distances at 3 m depth at the $P_{c\text{-net}}$ value of 244 kPa. The $\sigma_{r\text{-net}}$ and the ΔU values are normalized with the $P_{c\text{-net}}$ values. The radial distances, the r values, are normalized with the initial radius of the grout bulbs, the r_0 values. The r_0 values for Case 1, Case 2 and Case 3 are 0.25 m, 0.35 m and 0.10 m respectively.

The $\sigma_{r\text{-net}}/P_{c\text{-net}}$ and the $\Delta U/P_{c\text{-net}}$ ratios have the trend of inversely proportional to the square of the normalized radial distances, the r/r_0 ratios. Equations 4 and 5 express the relationships between the $\sigma_{r\text{-net}}/P_{c\text{-net}}$ ratios and r/r_0 and that between the $\Delta U/P_{c\text{-net}}$ ratios and r/r_0 respectively,

$$\sigma_{r\text{-net}} / P_{c\text{-net}} = \alpha\,(r_0 / r)^2 \quad (4)$$

$$\Delta U / P_{c\text{-net}} = \beta\,(r_0 / r)^2 \quad (5)$$

where α is the total radial pressure factor and β is the excess pore pressure factor. The α and the β factors are 1 and 0.7 respectively. The trend lines in Figure 6 show that there is virtually no difference in the α and the β factors between Case 1 to Case 3. The size effect of the grout bulbs is insignificant.

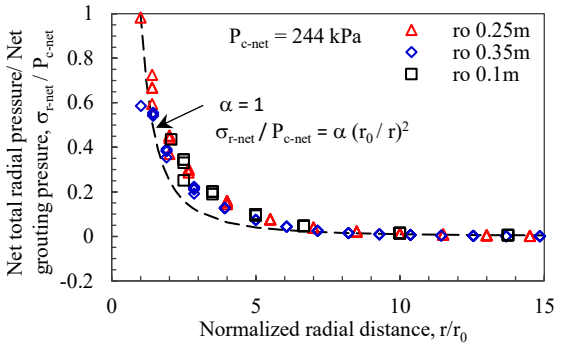

(a) Total radial pressures.

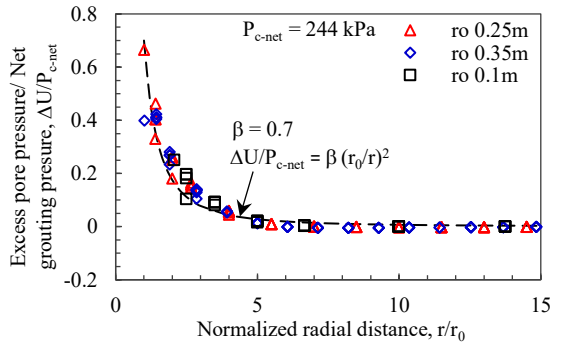

(b) Excess pore pressures.

Figure 6. Variation of radial pressures and pore pressures against radial distances.

4 SHEAR STRENGTH EFFECTS

4.1 *Distribution of Shear Stresses*

Figure 7 shows the distribution of the computed shear stresses, the τ values, under the net grouting pressure, $P_{c\text{-net}}$, of 724 kPa in the final stage for Case 1. The contours show that the peak τ values develop in conical surfaces at the upper and the lower semi-spheres of the grout bulb. The maximum τ values of -71.8 kPa and 61.4 kPa are initiated at the angles of 45° and 135° from the vertical axis along the grout-soil interface. The negative and the positive signs denote the opposite shearing directions.

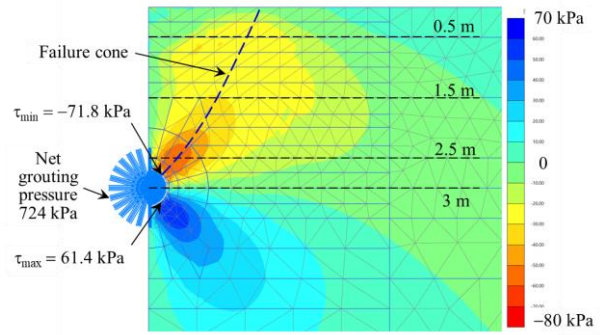

Figure 7. Contours of shear stresses in final stage of grouting - Case 1.

4.2 *Mobilization of Shearing Strengths*

Figure 8 presents the computed τ values occurring at Point 2, the lateral boundary of the grout-soil interface for Case 1 and Case 4. In the initial stages the τ values increase with the grouting pressures at the rate of $\tau/P_{c\text{-}net} = 0.36$. When the $P_{c\text{-}net}$ reaches the threshold value of 304 kPa, the τ value is fully mobilized to the s_u value of 60 kPa at the lateral Point 2 for Case 1. For Case 4, when the $P_{c\text{-}net}$ reaches the threshold value of 544 kPa, the τ value is fully mobilized to the s_u value of 120 kPa at the lateral Point 2. The threshold $P_{c\text{-}net}$ values are approximately $5s_u$ and $4.5s_u$ for Case 1 and Case 4 respectively.

The computed τ values exceeding the s_u value of 60 kPa at the $P_{c\text{-}net}$ values larger than 664 kPa for Case 1 are the sign of soil failure. Similarly for Case 4, failure occurs at the $P_{c\text{-}net}$ values exceeding 904 kPa for soil having the s_u value of 120 kPa. As shown in Figures 9 and 10, the peak shear stresses, the τ_{peak} values, at 2.5 m depth are within the undrained shear strength of 60 kPa at short radial distances to the interface.

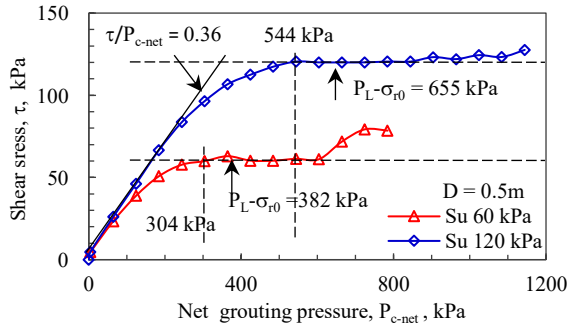

Figure 8. Computed shear stresses at the lateral grout-soil interface.

4.3 *Comparison with Simplified Solution*

The analytical solution for spherical cavity expansion adopts the elastic-plastic model to simplify the derivation of the equations. For spherical void expansion, Carter et al. (1986) provided the simplified solution for the limit pressure, P_L, which expressed in Equation 6:

$$P_L - \sigma_{r0} = 4/3\ s_u\ [1 + \ln (G/ s_u)] \quad (6)$$

The G value is the shear modulus of soil in the linear elastic-plastic model. The $P_L - \sigma_{r0}$ value is defined as the cavity pressure that induces the volume strain, $\Delta V/V_0$, equal to 1. At $\Delta V = V_0$, the shear stress in the plastic zone of the soil surrounding the void is fully mobilized to the undrained shear strength.

To compare the numerical results with those obtained by Equation 6, the secant shear modulus, the G_{50} value, is interpreted at $\varepsilon_{v\text{-}50}$, the volume strain mobilizing the 0.5 ($P_L - \sigma_{r0}$) value. Equation 7 defines the G_{50} as:

$$G_{50} = 0.5\ (P_L - \sigma_{r0}) / \varepsilon_{v\text{-}50} \quad (7)$$

Based on Figure 3, the $P_L - \sigma_{r0}$ value at $\Delta V/V_0 = 1$ is 700 kPa. At $0.5(P_L - \sigma_{r0})$, the $\varepsilon_{v\text{-}50}$ is 0.132 and the G_{50} is 2650 kPa. Using Equation 6, the $P_L - \sigma_{r0}$ for the s_u values of 60 kPa and 120 kPa are 382 kPa and 655 kPa respectively.

As indicated in Figure 8, the computed τ value reaches the ultimate value of 60 kPa at the threshold $P_{c\text{-}net}$ value of 304 kPa, which is close to the $P_L - \sigma_{r0}$ value of 382 kPa for Case 1. Similarly, the computed τ value reaches the ultimate value of 120 kPa at the threshold $P_{c\text{-}net}$ value of 544 kPa, which is close to the $P_L - \sigma_{r0}$ value of 655 kPa for Case 4. The analysis results using the HSS and the elastic-plastic models are consistent with each other.

4.4 *Failure Mechanism*

To examine the failure mechanism of the soil surrounding the grout bulb, the computed τ values along 3 horizontal sections at the depths of 0.5 m, 1.5 m and 2.5 m in the later grouting stages are extracted. Figure 7 depicts the locations for these 3 sections. Figure 9 presents the computed τ values for Case 1 under the $P_{c\text{-}net}$ values of 304 kPa, 484 kPa and 724 kPa at these 3 sections. In the final stage with the $P_{c\text{-}net}$ value of 724 kPa, the computed τ have the peak values of 30.0 kPa, 30.5 kPa and 59.0 kPa at 0.5 m, 1.5 m and 2.5 m depths respectively. Figure 10 presents the computed τ values under the $P_{c\text{-}net}$ values of 604 kPa, 844 kPa and 1144 kPa for Case 4. In the final stage with the $P_{c\text{-}net}$ value of 1144 kPa, the computed τ have peak values of 22.1 kPa, 35.1 kPa and 105.2 kPa at 0.5 m, 1.5 m and 2.5 m depths respectively. Figure 9 and Figure 10 show that as the $P_{c\text{-}net}$ values increase, the increase in the τ values propagate upward along the conical shearing surface shown in Figure 7.

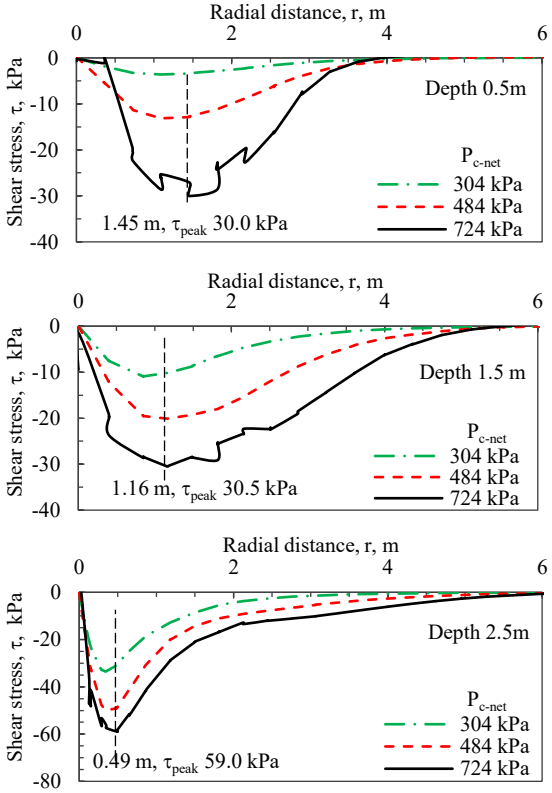

Figure 9. Computed shear stresses under various grouting pressures at depths of 0.5 m, 1.5 m and 2.5 m - Case 1.

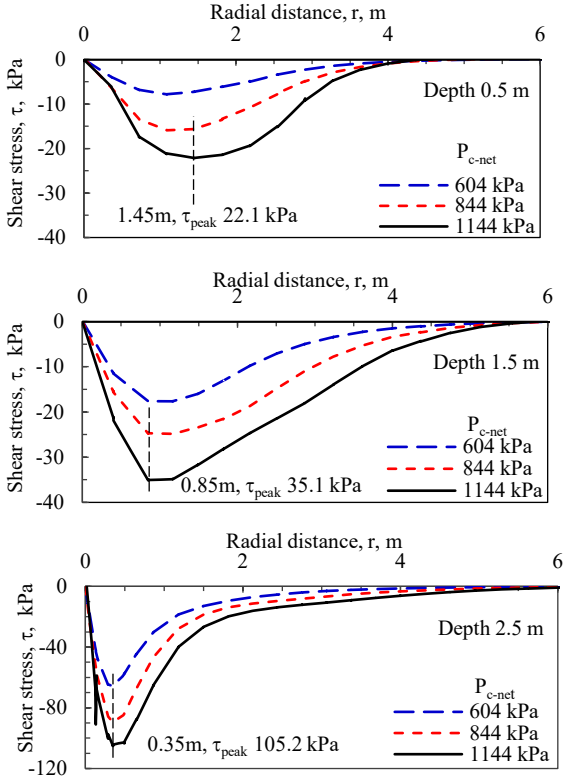

Figure 10. Computed shear stresses under various grouting pressures at depths of 0.5 m, 1.5 m and 2.5 m - Case 4.

4.5 *Failure Cone*

Figure 9 shows that the peak τ values are located at the radial distances of 0.49 m, 1.16 m and 1.45 m for the sections at 2.5 m, 1.5 m and 0.5 m depths respectively for Case 1. For Case 4, Figure 10 shows that the peak τ values are located at the radial distances of 0.35 m, 0.85 m and 1.45 m for those 3 sections respectively. Figure 11 plots the 2 trajectories of the peak shear stresses intersecting the 3 horizontal sections for Case 1 and Case 4. The envelop interpreted for these 2 shearing surfaces has an inclination around 30° from the vertical.

The failure cone inferred from the shear stress contours in Figure 7 is refined in Figure 11. In 3-Dimensional, the shearing surface resembles a 60-degree failure cone. Based on inclinometers monitoring on compaction grouting case histories, Graf (1969), Hwang & Moh (1994) and Wong et al. (1996) observed the 30-degree inclination of the conical shearing surface. The results of this numerical analysis verify that cone failure mechanism.

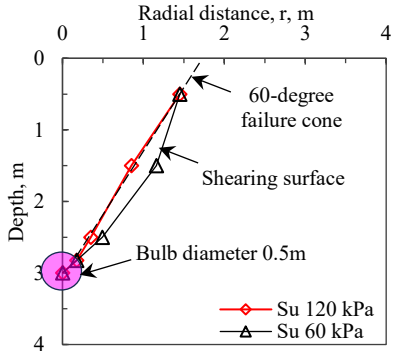

Figure 11. Distribution of peak shear stresses in final stage of grouting.

5 COMPUTED HEAVES

5.1 *Heave Profiles*

Figure 12 presents the computed heave profiles for Case 1 and Case 2. Figure 12(a) presents the computed δ_v values occurring at the $P_{c\text{-}net}$ values ranging from 364 kPa to 604 kPa for Case 1. For Case 2, Figure 12(b) shows the computed δ_v values at the $P_{c\text{-}net}$ values ranging from 244 kPa to 444 kPa. The maximum heaves, the $\delta_{v\text{-}max}$ values, under the same $P_{c\text{-}net}$ value of 364 kPa above the centres of the grout bulbs, are 0.28 mm and 1.06 mm for Case 1 and Case 2 respectively.

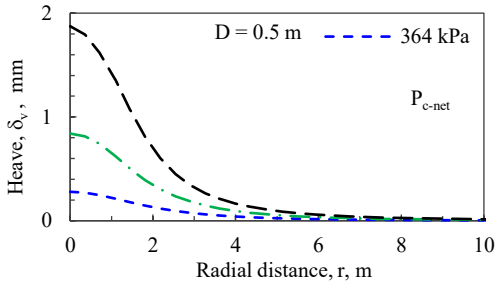

(a) Case 1 – Bulb diameter 0.5m.

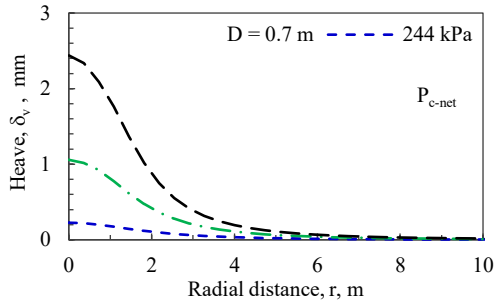

(b) Case 2 - Bulb diameter 0.7m.

Figure 12. Computed heave profiles for various grouting pressures.

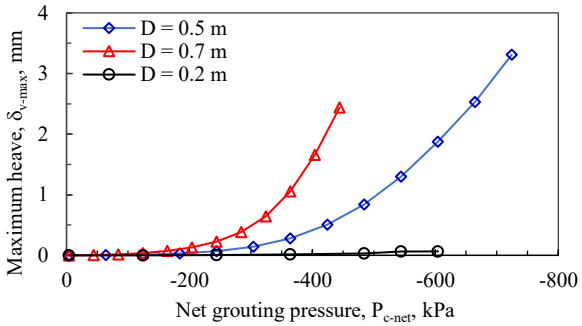

Figure 13. Maximum ground heave induced by compaction grouting.

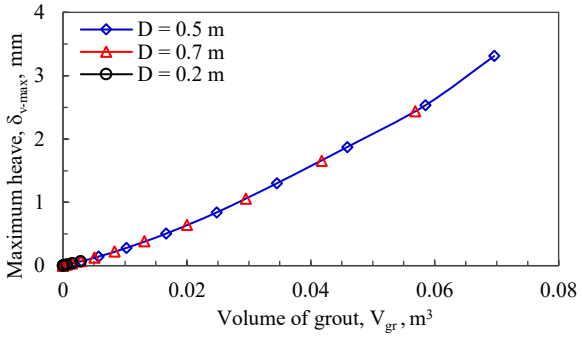

Figure 14. Computed heave induced by various grout bulb diameters.

Figure 13 shows the computed $\delta_{v\text{-}max}$ values under various $P_{c\text{-}net}$ values for Case 1 to Case 3. It appears that the larger the bulb diameter, the larger heaves would occur under the same grouting pressure. Figure 14 however shows that the heaves are directly proportional to the grout volumes, V_{gr} . The size effect to the performance of heave is insignificant.

The volumes of heave, the V_{he} values, for the computed heave profiles for the undrained Case 1 to Case 4 are related to the V_{gr} values. The V_{he} /V_{gr} ratios range from 0.97 and 0.99. Such ratios are close to unity.

5.2 *Normalized Heave Profiles*

The heave profiles presented in Figure 12(a) are normalized with the maximum heave values of the respective profiles. Figure 15 shows the normalized heave profiles for Case 1. The various normalized profiles merge into a common envelop. The normalized heave profiles for Case 2 are quite similar with those for Case 1 and not presented for clarity.

The Student's T-distribution function, as expressed in Equation 8, could match with the normalized heave profiles:

$$\delta_v / \delta_{v\text{-}max} = [1 + (r/\sigma)^2 / \nu\ ]^{-(\nu + 1)/2} \qquad (8)$$

where in this study δ_v is the heave at the radial distance r measuring from the vertical axis of the grout bulb and σ is the width of the heave profile at the point of inflection. The σ value is the standard deviation of the normal distribution in the probability and statistical analyses field. The ν value is the degree of freedom in Student's T-distribution.

The σ value is also the i value that Peck (1969) adopted in settlements estimation in tunnelling. Curve fitting on the normalized heave profiles shown in Figure 15 gives the σ values ranging from 1.4 m to 1.8 m and the ν value of 2. For sake of clarity, Figure 15 shows the T-distribution curves with the mean value of σ = 1.6 m and ν = 2. Relating to the depth of the grout bulbs, Z, of 3 m, the σ/Z ratio is around 0.53.

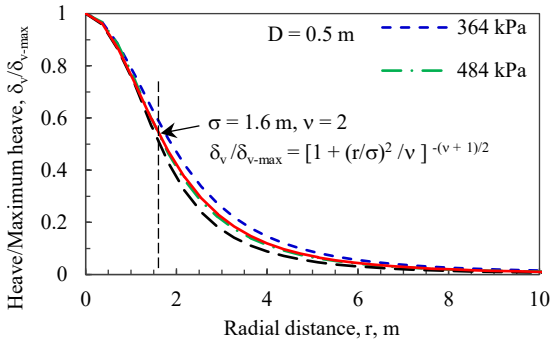

Figure 15. Normalized heave profiles induced by grouting pressures.

6 CONCLUSIONS

The Author has conducted the axisymmetric 2-Dimensional numerical analyses to study compaction grouting. The cases studied have the grout bulbs of 0.2 m, 0.5 m and 0.7 m in diameters located at the depth of 3 m. The analysis adopts the spherical cavity expansion method and the undrained soil material. The conclusions comprise the following:

(1) The effect of the grout bulb diameters on the performance of compaction grouting in terms of ground heaves and volume strains is insignificant.

(2) Generation of excess pore pressures plays a dominating role in the performance of compaction grouting. The computed excess pore pressures generated at the grout-soil interface are around 0.7 times the net grouting pressures.

(3) The computed total radial pressures at the grout-soil interface are equal to the net grouting pressures.

(4) The computed net effective radial pressures at the grout-soil interface are around 0.3 times the net grouting pressures.

(5) The variation of the total radial pressures is inversely proportional to the square of the normalized radial distances to the centre of the grout bulb.

(6) The distribution of the peak shear stresses above the grout bulb has an inclination of 30 degrees from the vertical. The failure mechanism of compaction grouting resembles a 60-degree failure cone.

(7) Mobilization of the shearing strength along the failure cone surface commences at the threshold net grouting pressures ranging from 4.5 to 5 times the undrained shear strengths of the surrounding soil.

(8) The limit grouting pressures inducing the ultimate shear stresses computed by numerical analysis using the nonlinear Hardening-soil with small-strain stiffness soil model are consistent with those estimated by the simplified solution using the elastic-plastic soil model.

(9) The volume of heave is equal to the volume of grout.

(10) The heave profiles have the Student's T-distribution. The degree of freedom is 2 and the widths at the points of inflection range from 1.4 m to 1.8 m.

The parametric studies conducted on compaction grouting show that the numerical tool can explore the complicate geotechnical problem. To enhance its application, further studies shall include the depth effects of the grout bulbs. The analyzed results shall compare with field observations for validation.

7 ACKNOWLEDGEMENTS

The Author wishes to express his sincere gratitude to Dr R.N. Hwang for his invaluable advices on the studies presented in this paper.

8 REFERENCES

Benz, T. 2006. Small-strain stiffness of soils and its numerical consequence. Dissertation of thesis, the Institute of Geotechnics, University Stuttgart.

Carter, J.P., Booker, J.R. & Yeung, S.K. 1986. Cavity expansion in cohesive frictional soils. *Geotechnique*, 36, No. 3: 349-358.

Graf, G.D. 1969. Compaction grouting technique and observations. *Journal of the Soil Mechanics Foundation Division*. ASCE. Vol.95, No. SM5, Sept:1151-1158.

Moh, Z.C., Yang, G.R. & Hwang, R.N. 1994. Response of soft soil to compaction grouting. *Proc., International Symposium on Structures and Foundations*, Hangzhou, China:30-56.(in Chinese)

Peck, R.B. 1969. Deep excavations and tunnelling in soft ground. *State of the Art Volume, 7th International Conference on Soil Mechanics and Foundation Engineering*, Mexico:225-290.

PLAXIS B.V. 2013. *PLAXIS Reference Manual*. PLAXIS, BV, Delft, the Netherlands.

Schanz, T. & Vermeer, P.A. 1998. On the Stiffness of Sands. *Geotechnique*, 46, No. 1: 145-151.

Schanz, T., Vermeer, P.A. & Bonnier, P.G. 1999. The hardening soil model: formulation and verification. *Beyond 2000 in Computational Geotechnics*. Rotterdam, the Netherlands:281-290.

Wong, L.W. & Chen, H.T. 1997. Fracture grouting for correcting building settlement. Proc., 2nd International Symposium on Structures and Foundations in Civil Engineering, Hong Kong:275-280

Wong, L.W., Shau. M.C. & Chen, H.T. 1996. Compaction grouting for correcting building settlemnt. *Grouting and Deep Mixing, Yonekura, Terashi & Shibazaki (eds)* @ 1996 Balkema, rottadam. ISBN 90 4410 805 3: 231-236.